A Juno-era View of Electric Currents in Jupiter's Magnetodisk

Z.-Y. Liu[1], M. Blanc[2,3], Q.-G. Zong[1,4]

[1]Institute of Space Physics and Applied Technology, Peking University, Beijing, China
[2]IRAP, CNRS-Universite Toulouse III Paul Sabatier, Toulouse, France
[3]LAM, Pytheas, Aix Marseille Universite, CNRS, CNES, Marseille, France
[4]MNR Key Laboratory for Polar Science, Polar Research Institute of China, Shanghai, China

Key Points:

- Four years of Juno magnetic field data are examined to delineate the currents in Jupiter's magnetodisk in the midnight-to-dawn sector.
- The radial current and the field-aligned current associated with it are consistent with the corotation enforcement model.
- The azimuthal current decreases as the local time increases, leading to a field-aligned current emptying the magnetodisk at pre-dawn.

Corresponding author: Q.-G. Zong and M. Blanc, qgzong@pku.edu.cn and michel.blanc@irap.omp.eu

Abstract

Recent observations from Juno provided a detailed view of Jupiter's magnetodisk, including its magnetic fields, waves, plasmas and energetic particles. Here, we contribute to Juno results by determining the electric currents threading the magnetodisk and their coupling to field-aligned currents (FAC) in the midnight-to-dawn local time sector. We first derive from Juno magnetic field data the spatial distributions of the height-integrated radial (I_r) and azimuthal (I_a) currents in the magnetodisk, and then calculate the FACs from the divergence of the two current components. The I_r-associated FAC, J_r, flows into and out of the magnetodisk at small and large radial distances, respectively, approximately consistent with the axisymmetric corotation enforcement model. On the other hand, I_a decreases with increasing local time everywhere in the local time sector covered, indicating an additional FAC (J_a) flowing out of the magnetodisk. From I_a and J_a, we conclude that the influence of the solar wind, which compresses the dayside magnetosphere and thus breaks the axisymmetry of currents and fields, reaches deep to a radial distance of at least 20 Jupiter radii. Our results provide observational constraints on Jupiter's magnetosphere-ionosphere-thermosphere coupling current systems, on their relation to the main auroral emission and on the radial mass transport rate in the magnetodisk, which we estimate to be close to ∼1500 kg/s.

1 Introduction

Jupiter has the largest magnetosphere among the planets in the solar system. Its magnetosphere is dominated by plasma originating from the moon Io, which orbits Jupiter at about 5.9 R_J (Jupiter radii, about 71,400 km) and supplies about 1-ton plasma per second to the magnetosphere [e.g. *Thomas et al.*, 2004; *Delamere et al.*, 2005]. The fresh Iogenic plasma injected into the magnetosphere as a result of ionization of Io torus neutral particles is picked up by the corotating electric field and dragged into corotation with Jupiter. The resulting centrifugal force drives, via interchange of flux tubes [*Hill*, 1976; *Southwood and Kivelson*, 1987], a strong outward radial transport of Iogenic plasma to large Jovicentric distances, stretching magnetic field lines near the centrifugal equator and generating an extended magnetodisk at all local times. This magnetic field configuration is supported by an azimuthal current disc [*Hill and Michel*, 1976] confined near the equator in the middle and outer magnetosphere [e.g. *Smith et al.*, 1976; *Khurana*, 2001; *Liu et al.*, 2021]. Models of the configuration of this magnetodisk, which have

clarified the relative contributions of the centrifugal force, plasma pressure gradient force and pressure anisotropy force to its equilibrium, have been developed first by *Caudal* [1986] and more recently by *Nichols et al.* [2015] and *Millas et al.* [2023]. The Jovian magnetodisk is rather thin compared to its horizontal extent: in the midnight-to-dawn local time sector, it extends horizontally from ∼20 R_J to ∼100 R_J, whereas in the vertical direction its half-thickness is only ∼1-2 R_J in general [e.g. *Khurana et al.*, 2022; *Liu et al.*, 2021].

When flowing outward, the plasma angular velocity decreases as a result of the Coriolis force, which works to conserve angular momentum in the flow and drives an outward radial current in the disk. The net divergence of this radial current in turn generates, in a steady state case, a third component of electric currents associated to the disk: a system of magnetic-field-aligned currents which flow into or out of the two conjugate ionospheres and close horizontally inside their conducting layers. Overall, the global current system generated by the outflow of Iogenic plasma transfers angular momentum between the magnetodisk and the upper atmosphere of the planet, thus fully or partly maintaining corotation of the magnetodisk with the planet. Finally, magnetic field lines threading the magnetodisk are drawn out of the meridian plane into a a sweep-back configuration under the effect of the radial current, as described by *Khurana and Kivelson* [1993]. This current produces a J×B force towards the east that tends to accelerate the plasma back toward corotation.

This description, commonly referred to as the corotation enforcement model, focuses solely on the concurrent roles of internal sources of plasma (Io) and momentum (planetary rotation) in shaping the magnetodisk configuration and its three associated current systems. It was initially formulated by *Hill* [1979] and later developed in detail and used for predictions at Jupiter [*Cowley and Bunce*, 2001; *Hill*, 2001; *Ray et al.*, 2014]. One of its main merits has been to provide a successful explanation of the Jovian main aurora, as departures of magnetospheric plasma flows from rigid corotation are observed at radial distances mapping along field lines to the location of the main auroral emission. However, this interpretation of the main aurora has been recently challenged on the basis of Juno and other observations by *Bonfond et al.* [2020], who showed that it displays significant azimuthal, inter-hemispheric and temporal variations and has been proven to be influenced by solar wind conditions [e.g. *Gurnett et al.*, 2002; *Yao et al.*, 2019, 2022].

Thus there is no doubt that the effects of solar wind interactions with the Jovian magnetosphere should be added to this picture. *Southwood and Kivelson* [2001] analyzed the consequences of the time-dependent contractions and expansions of the dayside magnetosphere by the solar wind pressure, which are expected to produce strong local-time asymmetries (particularly dayside-nightside) in plasma flows, current systems and auroral features: see the review of these local time asymmetries by *Arridge et al.* [2016]. *Khurana* [2001] showed from the analysis of night-side Galileo magnetic field data that magnetodisk radial and azimuthal currents both display strong local time asymmetries and both contribute to the generation of field-aligned currents. In their view, the divergence of azimuthal currents at dawn and dusk they deduced from Galileo observations feeds an additional field-aligned current system, superposed to the corotation enforcement one, that results from solar wind control effects deep into the magnetosphere. *Khurana et al.* [2022] later determined quantitatively the magnetodisk thickness, confirming that it is significantly larger on the dusk-side than on the night-side. They interpreted this feature as the effect of a single Dungey-type circulation cell generating a region of open magnetic flux confined to the dawn-side magnetosphere.

There is currently no consensus on how the solar wind interaction influences internal magnetospheric dynamics: see again *Arridge et al.* [2016]. One view is that it results from merely internal processes modulated by the confinement of plasma flows inside a strongly asymmetric magnetospheric cavity [*Delamere and Bagenal*, 2010]. The other one is that Jovian and interplanetary magnetic fields reconnect over a limited area of the magnetopause on the dawnside, producing there a domain of open flux that distorts the configuration and flows of the magnetodisk and the corresponding auroral features. Both scenarios predict dawn-dusk and noon-midnight asymmetries in magnetodisk and field-aligned currents that need to be informed by direct observations. In this context, determination of the actual current systems linked to the magnetodisk is of the utmost interest. In his pioneering work, *Khurana* [2001] determined the basic morphology of these current systems on the nightside from Galileo data and revealed their dawn-dusk asymmetry. More recently, *Lorch et al.* [2020] extended this work to all local times. Using all magnetic field data available from space missions until July 2018, including a first set of Juno orbits, they calculated magnetodisk and field-aligned current systems at all local times, mainly confirming the existence of a significant divergence of azimuthal currents

and the importance of their determination for future studies of magnetosphere-ionosphere-thermosphere (MIT) coupling at Jupiter.

Magnetospheric science with Juno [*Bagenal et al.*, 2017] has revolutionized our understanding of many open questions. Thanks to its unique eccentric polar orbit, it has provided new insight into the ionospheric component of MIT coupling current systems. Juno observations of the auroral and polar ionosphere not only confirmed the persisting existence of field-aligned currents, but also provided for the first time direct measurements of their magnitude and spatial distributions [*Kotsiaros et al.*, 2019]. They revealed a large north-south asymmetry in the magnitude of FACs, with northern FAC amplitudes being about half of southern FAC ones.

Furthermore, development for Juno of a multi-instrument method linking UV and IR spectro-imaging observations of the main auroral emission to in-situ magnetic field and electron precipitation observations made it possible to retrieve simultaneously the ionospheric components of field-aligned and horizontal currents that close the giant current loop connecting the magnetodisk to the ionosphere-thermosphere [e.g. *Wang et al.*, 2021; *Al Saati et al.*, 2022]. It revealed that, although in the southern hemisphere the upward FACs are always located equatorward of the downward FACs, the pattern for the northern hemisphere is more complex. In about 70% of the northern flybys studied by *Al Saati et al.* [2022], upward FACs are located on the equatorward side as well, while in the other northern flybys the opposite trend was observed. The latter trend indicates that the northern ionospheric plasma might be temporally in super-corotation, a phenomenon noted previously when studying the equatorial magnetic fields measured by Voyager 1 and 2 [*Hairston and Hill*, 1986].

In this paper, we contribute to the determination by Juno of the different interconnected components of the magnetosphere-ionosphere-thermosphere (MIT) coupling current systems at Jupiter. We determine from Juno magnetic field data alone the current system threading the magnetodisk and its coupling to field-aligned currents in the midnight-to-dawn local time sector covered by Juno during its prime mission. We first establish a spatial distribution of the height-integrated perpendicular current density $I_{\perp}$ in the magnetodisk, using Juno/MAG [*Connerney et al.*, 2017; *Connerney*, 2017] observations of the magnetic fields during 404 magnetodisk crossings in the night-to-dawn sector identified by *Liu et al.* [2021]. Then, using current continuity, we determine FACs

from the divergence of $I_{\perp}$. The FACs obtained highlight the contribution of azimuthal currents and allow one to divide the magnetodisk into three sub-regions with respect to their sign. In the remainder of the paper, we first describe the materials and methods (section 2), then present our results (section 3), and finally discuss them by comparison with previous publications (section 4).

2 Materials and method

2.1 Juno Observations of magnetodisk Crossings

Because of Jupiter's rotation and dipole tilt, Juno crosses the magnetodisk periodically. Figure 1a shows a representative crossing on August 30, 2017. The top three panels give the three components (B_x, B_y and B_z) of the magnetic fields in the JSO coordinate system during the crossing, whereas the fourth panel shows the magnitude (B_t). Before the crossing, Juno is located in the southern lobe, as indicated by the positive B_x and B_y. Then, Juno approaches the magnetodisk, showing as B_x, B_y and B_t gradually decrease to zero. Finally, B_x and B_y continue to decrease before reaching their most negative values, while B_t returns to its pre-crossing value, signaling the entry of Juno into the northern lobe.

To analyze the crossing in a more appropriate reference frame, we transform the magnetic field into an LMN coordinate system, which is a local current sheet coordinate system determined by a minimum variance analysis (MVA) [*Sonnerup and Scheible*, 1998; *Liu et al.*, 2021] of the observed field. The L axis of this coordinate system (denoted by x_l, increasing outward) corresponds to the component of the magnetic fields changing most during crossings. According to the geometry of the magnetodisk [e.g. *Khurana and Kivelson*, 1989; *Khurana*, 1992], it represents the direction of the lobe magnetic field. As shown in Figure 3 of *Liu et al.* [2021], this direction is roughly radial at small radial distances to Jupiter and gradually rotates towards the azimuthzal direction as radial distance increases. The N axis (denoted by x_n, increasing upward) corresponds to the direction along which the magnetic field changes most, or in other words, the direction of the gradient. This direction can be regarded as the normal to the magnetodisk. Finally, the M axis (denoted by x_m, increasing eastward) completes the right-handed coordinates. As we will show in the following subsection, currents in the magnetodisk approximately flow in this direction. The bottom three panels of Figure 1a present the magnetic field in

the LMN coordinate system. Consistent with the definition above, most changes are seen in B_l, which is about -20 nT before the crossing, becomes zero near the magnetodisk center, and approaches about $+20$ nT at the end. On the other hand, B_n and B_m do not vary much during the whole crossing.

2.2 Height-integrated Perpendicular Current Density $I_\perp$

Next, we compute $I_\perp$ from the observed magnetic field profile. This can be done most easily in the LMN coordinates. To see this, we first write down the three components of the current density (j_l, j_m and j_n) in terms of the magnetic field by virtue of Ampere's law (neglecting displacement current)

$$\begin{cases} j_l = \frac{1}{\mu_0}\left(\frac{\partial B_n}{\partial x_m} - \frac{\partial B_m}{\partial x_n}\right) \\ j_m = \frac{1}{\mu_0}\left(\frac{\partial B_l}{\partial x_n} - \frac{\partial B_n}{\partial x_l}\right) \\ j_n = \frac{1}{\mu_0}\left(\frac{\partial B_m}{\partial x_l} - \frac{\partial B_l}{\partial x_m}\right) \end{cases}, \tag{1}$$

where μ_0 denotes the permeability of vacuum. Recalling the definition of the LMN coordinates, we have the ordering $\frac{\partial}{\partial x_m} \sim \frac{\partial}{\partial x_l} \ll \frac{\partial}{\partial x_n}$. One can see that j_n is much smaller than j_m. j_l should be much smaller than j_m as well. On the one hand, the first term of j_l is negligible according to the above ordering. On the other hand, since the variation of B_m between the two lobes is much smaller than that of B_l (which is also a property of the LMN coordinates), the second term of j_l is also small compared to the first term of j_m. Thus, the total current density $\vec{j}$ can be reduced to $\vec{j} \approx j_m \hat{x}_m$, where $\hat{x}_m$ represents a unit vector in the M direction.

Further, following from the LMN ordering, the second term of j_m should be much smaller than the first term. This statement can be tested directly by observations. As an estimate, we take $\frac{\partial B_l}{\partial x_n} \sim \frac{B_l}{H}$ and $\frac{\partial B_n}{\partial x_l} \sim \frac{\partial B_n}{\partial r}$, where r represents the radial distance to Jupiter and H the half-thickness of the magnetodisk. Taking these quantities from *Liu et al.* [2021] (their Figure 2 for H and Figure 4 for B_n and B_l as a function of r), we obtain $|\frac{\partial B_n}{\partial x_l}|/|\frac{\partial B_l}{\partial x_n}| < 5\%$, supporting the above assertion of j_m. Therefore, we can finally write

$$\vec{j} \approx j_m \hat{x}_m \approx \frac{1}{\mu_0}\frac{\partial B_l}{\partial x_n}\hat{x}_m. \tag{2}$$

This equation suggests that currents in the magnetodisk are approximately in the M direction and primarily depend on B_l.

On the basis of Equation (2), we define $I_\perp$ explicitly in this study as

$$I_\perp = \int j_m dx_n = \frac{1}{\mu_0} \int \frac{dB_l}{dx_n} dx_n = \frac{1}{\mu_0}(B_{l,n} - B_{l,s}), \tag{3}$$

where $B_{l,n}$ and $B_{l,s}$ represent the magnetic fields in the northern and southern lobes, respectively. To extract $B_{l,n}$ from observations, we first identify the zero point of B_l in each crossing. Then, we isolate a one-hour interval before or after the zero point (depending on the direction of the crossing) when Juno is located in the northern lobe. Finally, we calculate the 95th percentile of B_l in this one-hour interval, and take it as $B_{l,n}$. $B_{l,s}$ is obtained similarly. For the example shown in Figure 1a, $B_{l,n}$ and $B_{l,s}$ obtained in this way are marked by the blue and red dashed lines in the bottom panel, respectively. One can see that they capture well the features of the lobe magnetic fields.

We then apply this method to the 404 magnetodisk crossings identified by *Liu et al.* [2021], which provides a spatial distribution of both the magnitude ($I_\perp$) and direction ($\hat{x}_m$) of the magnetodisk currents.

2.3 Field-aligned Current Density $J_\parallel$

Since the total current system has to be divergence-free, the FACs are related to the divergence of the magnetodisk currents. To calculate the latter, we have to transform the current density obtained in the LMN coordinates, which varies from crossing to crossing, to a global reference frame chosen to be the same for all crossings. Strictly speaking, this calculation of magnetodisk current divergence must take into account the non-planar shape of the magnetodisk mean position, as described by [e.g. *Kivelson et al.*, 1978; *Khurana*, 1992]. Fortunately, Juno observations suggest several simplifications. First, all crossings are observed near the JSO x-y plane, since their JSO latitudes, shown in Figure 2a, are very close to zero. Second, the lobe magnetic fields are approximately parallel to the JSO x-y plane. As shown in Figure 2b, in most crossings the angle of the L axis to the JSO x-y plane is close to zero. These two results suggest that magnetodisk crossings are well confined to the JSO x-y plane. Finally, Figure 2c shows that the angle from the M axis to the JSO x-y plane is generally small (see the black curve representing its average level), though some low-amplitude scatter is present. Taken altogether, inspection of the parameters plotted in Figure 2 suggests that magnetodisk currents are approximately aligned with the JSO x-y plane. This allows us to use in the remainder of this study the simplifying assumption that the magnetodisk and its embedded currents

are approximately confined to the JSO x-y plane, and to adopt a cylindrical coordinate system using the JSO z-axis as its polar axis. The relative error of this approximation can be estimated to be $(1 - \cos\alpha) \sim 12\%$, where α represents the angles between relevant quantities and the JSO x-y plane estimated from Figure 2. In the following, we will see that this error is comparable with the statistical uncertainty in $I_\perp$ caused by temporal variations, which suggests it is acceptable.

Transformation of magnetodisk currents from the LMN coordinates to the global reference frame is straightforward. The magnitude is still $I_\perp$, whereas the direction is given by the projection of $\hat{x}_m$ onto the JSO x-y plane (a direction which is almost entirely determined by the L axis). Figure 1b shows how magnetodisk currents are distributed in the global reference frame, with colors giving their magnitude and the short lines giving their direction. Three features emerge: (1) At any given local time (ϕ), $I_\perp$ decreases as the radial distance to Jupiter (r) increases. (2) At a fixed r, $I_\perp$ decreases as ϕ increases. (3) At small r, magnetodisk currents are primarily in the azimuthal direction, and their radial component tends to increase with increasing r.

Using the aforementioned definitions and approximation, we can now compute the divergence of magnetodisk currents. Since a cylindrical coordinate system is adopted here, we decompose these currents into their radial (I_r) and azimuthal (I_a) components, as illustrated in Figure 1c. In this way, one can write that the total current divergence vanishes as:

$$J_{\parallel,n} + J_{\parallel,s} = \frac{1}{r}\frac{\partial(rI_r)}{\partial r} + \frac{1}{r}\frac{\partial I_a}{\partial \phi}, \tag{4}$$

where $J_{\parallel,n}$ and $J_{\parallel,s}$ denote the FACs flowing between the magnetodisk and the northern and southern ionosphere, respectively. As mentioned in the Introduction, Juno observations show that these two quantities are generally unequal [*Kotsiaros et al.*, 2019; *Al Saati et al.*, 2022]. In the absence of direct information on their relative amplitudes in the data used for this study, we deal only with their average, $J_\parallel = \frac{1}{2}(J_{\parallel,n} + J_{\parallel,s})$. One can easily obtain $J_{\parallel,n}$ and $J_{\parallel,s}$ from $J_\parallel$ by specifying a ratio of $J_{\parallel,s}$ to $J_{\parallel,n}$.

Further, for the sake of discussion, we designate two additional variables representing the relative contributions of I_r and I_a to $J_\parallel$, $J_r = \frac{1}{2}\frac{1}{r}\frac{\partial(rI_r)}{\partial r}$ and $J_a = \frac{1}{2}\frac{1}{r}\frac{\partial I_a}{\partial \phi}$.

2.4 Mapping to Ionosphere

In order to be able to compare the field-aligned currents flowing out of the magnetodisk to their values observed in the ionosphere and polar magnetosphere by Juno, we map $J_{\parallel}$ along magnetic field lines to the ionosphere using the JRM33 model and the *Connerney et al.* [2020] magnetodisk model. First, we calculate the System III latitude (λ_{S3}) of the footprints of the crossings. Then we multiply $J_{\parallel}$ by a factor $\frac{B_i}{B_n}$ to obtain the ionospheric FACs $J_{\parallel,i}$, where B_i represents the magnitude of the magnetic fields at the ionosphere altitude.

By checking the resulting distributions, we find that $I_{\perp}$ is insensitive to the System III longitude of the crossings (ψ_{s3}). Therefore, the effects of ψ_{s3} can be neglected in most parts of this study. However, ψ_{s3} indeed significantly affects the mapping to the ionosphere, as λ_{S3} is not only a function solely of JSO coordinates but also of ψ_{s3}. The implication is that different crossings which are close to one another in JSO coordinates are taken at different time and thus different ψ_{s3}. Therefore, strictly speaking, there is no unique footprint latitude for $J_{\parallel}$. In order to reduce the effects of temporal variations between different crossings, $J_{\parallel}$ is computed statistically from an average of several crossings. This procedure works well for the southern ionosphere, where magnetic fields are regular. But it fails for mapping to the northern ionosphere due to the highly twisted magnetic fields there. Hence, in what follows, we only show $J_{\parallel,i}$ in the southern ionosphere. In addition, we note our procedure of projections may add some artificial latitude spread to the latitude profile of $J_{\parallel,i}$, as the field-aligned currents associated with the main aurora at different longitudes tends to map at different latitudes.

3 Results

3.1 Distributions of I_r and J_r

Figure 3a shows the distribution of I_r in the JSO x-y plane. Although there is a large scatter due to temporal variations, a trend of I_r increasing at small r and decreasing at large r with increasing r can be identified unambiguously. To focus on this trend, we group I_r into several bins according to ϕ. On the one hand, we would like to maximize the number of bins, to remove the effects of ϕ. On the other hand, to get enough samples in each bin, the number of bins should be as small as possible. Moreover, the ϕ distributions of samples in each bin should be relatively uniform. The best compromise is

to use three bins of ϕ spanning from 0 hr to 2 hr, from 2 hr to 4 hr, and from 4 hr to 6 hr. The three color-coded boxes in Figure 3a illustrate them.

Figure 3b shows the radial profile of I_r in different ϕ bins. Inside r =60 R_J, I_r increases as r increases regardless of ϕ. Outside r =60 R_J, I_r is only available within 4 hr< ϕ <6 hr. There, I_r shows a clear decreasing trend from r =60 R_J to r =80 R_J. An increasing trend is observed again at r >80 R_J. However, observations there might be contaminated by magnetopause currents. Thus, we do not discuss them further, although we still show them in the following figures for completeness.

Figure 3c shows J_r derived from I_r, with positive and negative values indicating FACs flowing into and out of the magnetodisk (i.e., out of and into the ionospheres), respectively. Inside r =80 R_J, the overall pattern of J_r agrees well with the axisymmetric corotation enforcement model. Namely, at small r, J_r is positive and flows into the magnetodisk, whereas at larger r, J_r becomes negative and flows out of the magnetodisk. However, the total into-magnetodisk and out-of-magnetodisk FACs per radian of azimuth are highly imbalanced, with the former and latter being 25.9±6.1 MA/rad and 2.9±5.2 MA/rad, respectively. This observation indicates that the whole current system cannot be closed solely with currents in the meridian plane. Instead, currents off the meridian plane must be involved to reach closure.

3.2 Distributions of I_a and J_a

Figures 3d-3f display I_a and J_a, with the same format as Figures 3a-3c. By comparing Figures 3a and 3d, we find that the magnitude of I_a ($\sim 10^3$ kA/R_J) is about one order of magnitude larger than I_r ($\sim 10^2$ kA/R_J), indicating I_a is the dominant component in terms of magnitude. Moreover, I_a has a spatial distribution similar to $I_\perp$. It also decreases as r and ϕ increase. The dependence on r and ϕ can be seen more quantitatively in Figure 3e, which shows I_a as a function of ϕ in four r bins.

The dependence of I_a on ϕ indicates the existence of nonzero J_a. Figure 3f displays J_a at different r. For the sake of presentation, this panel is divided into two sub-panels, with the top and bottom sub-panels showing J_a outside and inside r =40 R_J, respectively. Two features are noted. First, J_a is negative regardless of r, indicating a FAC flowing out of the magnetodisk. Second, the magnitude of J_a decreases sharply with increasing r.

Consequently, J_a is about twice the magnitude of J_r within 20 $R_J < r <$40 R_J, but becomes secondary at larger r, though $|J_r|$ itself also decreases as r increases.

3.3 Total FACs $J_\parallel$

Next, we combine J_r and J_a together to obtain $J_\parallel$. When calculating J_r and J_a, the coordinate space of interest ([20-100] $R_J \times$[0, 6] hr) is divided into $r \times \phi$ bins with different manners (7×3 for J_r and 4×4 for J_a). To compute $J_\parallel$, we first re-divide the whole space into 16×12 bins, then linearly interpolate J_r and J_a onto the new grids, and finally add them up. Figure 4a shows $J_\parallel$ in the JSO x-y plane, with the warm and cool colors representing $J_\parallel$ flowing from the conjugate ionospheres into the magnetodisk and from the magnetodisk into the conjugate ionospheres, respectively.

The local time coverage is highly limited by the geometry of Juno orbits. Hence, here we primarily focus on the radial distributions. Figure 4b shows $J_\parallel$ as a function of r within the 3.5 hr$< \phi <$4.5 hr sector, where the whole radial extent from 20 R_J to 80 R_J is well covered by Juno. In terms of the sign of $J_\parallel$, the magnetodisk can be divided into three subregions:

1. 20-40 R_J: $J_\parallel < 0$. J_a is dominant in this subregion, although J_r reaches its most positive value there.
2. 40-60 R_J: $J_\parallel > 0$. J_r and J_a are positive and negative, respectively. J_r is the dominant component in terms of magnitude in this subregion.
3. 60-80 R_J: $J_\parallel < 0$. Both J_r and J_a are negative there.

Interestingly, we note that *Szalay et al.* [2017] concluded to the existence of a similar three-sub-regions structure, based on plasma data taken by Juno/JADE [*McComas et al.*, 2017] during the first science perijove of Juno.

Figure 4b shows that the magnitude of $J_\parallel$ is about a few kA/R_J^2 in general. To better capture the global balance of FACs, we calculate the total into-magnetodisk ($I_{\parallel,+}$) and out-of-magnetodisk ($I_{\parallel,-}$) FACs per radian of azimuth by integrating $J_\parallel$ over corresponding radial extent. The results are $I_{\parallel,+}$ =6.8±3.2 MA/rad and $I_{\parallel,-}$ =10.4±4.3 MA/rad. Therefore, the total into-magnetodisk FACs are approximately balanced by the total out-of-magnetodisk FACs. There are no net FACs ($I_{\parallel,+} - I_{\parallel,-} = -3.6 \pm 5.4$

MA/rad) within the error range, which also implies that the divergence of radial magnetodisk currents is well balanced by that of azimuthal currents.

3.4 Ionospheric FACs $J_{\parallel,i}$

Finally, we map $J_{\parallel}$ to the southern ionosphere using the method described in section 2.5. Figure 4c shows the results. The most notable feature is the positive $J_{\parallel,i}$ spanning from the $\sim -70°$ latitude to the $\sim -78°$ latitude. As suggested by previous observations [e.g. *Grodent et al.*, 2003], this latitude range corresponds to the main auroral emission. Theoretical considerations generally attribute the main auroral emission to upward FACs [e.g. *Cowley and Bunce*, 2001]. Our results based on equatorial observations thus confirm this suggestion. In addition, they provide the equatorial location corresponding to the main auroral emission, that is, $\sim$40 $R_J < r < 60$ R_J.

4 Discussion

In this section we discuss our calculations of the different current systems threading the Jovian magnetodisk in the midnight-to-dawn sector in the light of their implication on global radial mass transport in the disk, and compare them with estimates of these current systems based on previous observations. Some implications of our results on our current understanding of MIT coupling at Jupiter are drawn.

4.1 Radial Mass Transport

As suggested by corotation-enforcement models [*Hill*, 1979; *Vasyliunas*, 1983; *Cowley and Bunce*, 2001], I_r results from the balance of torques associated with radial currents in the equatorial plane and latitudinal currents in the ionosphere. In the equatorial plane, the electrodynamic torque exerted by the J×B force balances the net transport of angular momentum carried by radial plasma motions, which can be written as [also see *Ray et al.*, 2014]

$$\dot{M}\frac{d}{dr}(r^2\omega) = 2\pi r^2 I_r B_n, \tag{5}$$

where ω represents the angular velocity and $\dot{M}$ denotes the radial mass transport rate. We note I_r has been estimated in this study, while B_n has been modeled by *Liu et al.* [2021] as $B_n = -2.3 \times 10^4 r^{-2.58}$ nT. Therefore one can obtain either ω or $\dot{M}$ by specifying the other quantity. Here, we choose to derive $\dot{M}$ from previous observations of ω.

The grey dots in Figure 5 show the flow speed derived from Juno/JADE ion measurements by *Kim et al.* [2020] (their Figure 6). The solid curves display the quantity $V_f = r\omega$ derived from Equation (5), or more explicitly,

$$V_f = \frac{r_0^2}{r}\Omega_J + \frac{1}{r}\frac{2\pi}{\dot{M}}\int_{r_0}^{r} r^2 I_r B_n dr, \tag{6}$$

where Ω_J is Jupiter's angular velocity (1.7735×10^{-4} rad/s) and r_0 is taken as 15 R_J, a radial distance where the magnetodisk is assumed to be in rigid corotation with the planet. One can see that the black curve corresponding to $\dot{M} = 1500$ kg/s approximately represents the median levels of the flow speed, whereas the red curve corresponding to $\dot{M} = 2000$ kg/s and the blue curve corresponding to $\dot{M} = 1000$ kg/s fit the upper and lower envelopes, respectively. From Figure 5, we conclude that a radial mass transport rate of ∼1500 kg/s matches Juno observations of the magnetodisk currents and flow speed best.

4.2 Comparison with Previous magnetodisk Current Observations

In light of their importance, electric currents in Jupiter's MIT coupling system have for two decades been broadly studied. In this subsection, we compare our results with three previous representative studies also based on magnetodisk observations: *Khurana* [2001], *Ray et al.* [2014] and *Lorch et al.* [2020]. The first two works were based on Galileo data, whereas the third one included all jovian missions and flybys before July 2018, including an early set of Juno orbits.

The radial profiles of I_r obtained by the three studies and ours show similar unimodal structures, although the detailed location of the peak is somewhat different (ranging from 30 R_J to 60 R_J). Besides, *Khurana* [2001], *Lorch et al.* [2020] and our study (also *Nichols and Cowley* [2022] who showed I_r in some particular cases) obtain similar magnitude of I_r. For example, all these studies find I_r of about 500 kA/R_J at r ∼50 R_J, ϕ ∼6 hr. However, the value of I_r given by *Ray et al.* [2014] is only about half of ours. This difference might be explained by the radial mass transport rate (∼1000 kg/s) used by *Ray et al.* [2014] to compute $I_\perp$, which is smaller than the value inferred from our observations (∼1500 kg/s).

Regarding J_r, the results obtained by our study are slightly different from the three previous papers. We find that J_r is negative within 60 $R_J < r <$80 R_J, while they showed

a positive J_r at all r in the midnight-to-dawn sector. However, the differences are small, as all four papers show $|J_r|$ within 60 $R_J < r <$80 R_J is close to zero.

Khurana [2001], *Ray et al.* [2014] and our study all investigated J_a and found that it flows from the magnetodisk into the ionosphere in the midnight-to-dawn sector. Our results especially highlight the effects of J_a at small r. Our Figure 4 shows that J_a dominates $J_\parallel$ within 20 $R_J < r <$40 R_J, and that the latter is directed from the magnetodisk to the ionosphere there. In contrast, *Khurana* [2001] and *Lorch et al.* [2020] found that $J_\parallel$ flows into the magnetodisk at all r. Consequently, in our picture, the into-magnetodisk FACs are roughly balanced by the out-of-magnetodisk FACs within the midnight-to-dawn sector, whereas *Khurana* [2001] and *Lorch et al.* [2020] required out-of-magnetodisk FACs at other local time (e.g., duskside) to close the into-magnetodisk FACs in the midnight-to-dawn sector.

4.3 Comparison with Juno Polar Observations

Finally, we compare our results with Juno observations of FACs over Jupiter's polar regions. Interestingly, the magnitude of $J_{\parallel,i}$ obtained in our study based on magnetodisk measurements is very close to those inferred from Juno polar measurements. *Kotsiaros et al.* [2019] analyzed magnetic field variations detected during Juno transits through polar regions. They estimated a total downward FAC integrated over azimuth of ∼58 MA in the southern hemisphere and ∼24 MA in the northern hemisphere, corresponding to a north-south averaged current density of ∼6.5 MA/rad that roughly agrees with ours ($I_{\parallel,-}$ =10.4±4.3 MA/rad).

By combining Juno multi-instrument data and modeling tools, *Wang et al.* [2021] and *Al Saati et al.* [2022] surveyed FACs and their other defined "MIT coupling Key Parameters" comprehensively during Juno magnetic footprint traversals of the main auroral emission. They found peak values of FACs (both upward and downward) in the northern and southern hemispheres of about 1 μA/m^2 and 2 μA/m^2, respectively. These results are comparable with our results shown in Figure 4c. In addition, assuming longitudinal homogeneity of currents for simplicity, *Wang et al.* [2021] estimated from the perijove 3 flyby that the total FAC entering/leaving the southern hemisphere is close to ∼66 MA, also consistent with our estimates.

However, two significant differences appear between our equatorial and these previous polar observations. First, the latter generally found a two-subregion structure with an upward FAC on the equatorward side and a downward FAC on the poleward side, except for a minor fraction of northern flybys for which *Al Saati et al.* [2022] observed the opposite trend. In contrast, our study finds an additional downward FAC on the equatorward side of the upward FAC. The absence of this additional downward FAC in polar observations might be explained by the different ranges of local time covered by Juno equatorial observations (the midnight to dawn quadrant) and polar observations (noon-dusk quadrant in the southern hemisphere, 15 to 21 LT for the northern hemisphere), as shown by figure 11 of *Al Saati et al.* [2022].

Another difference appears between the latitudinal width of the main region of upward currents estimated from the different studies: Figure 6 of *Al Saati et al.* [2022] shows that it is on the order of 2 degrees at most for the southern hemisphere, while in our study (figure 4c), the full width at half maximum of our FACs projected on the southern hemisphere is on the order of 5 degrees. This may be due to the LT variations in latitudinal width of the main auroral emission, or possibly to the slight dispersion in latitude produced by our projections of magnetodisk crossings at different longitudes (see our discussion in section 2.4). To resolve this discrepancy, future observations of polar and equatorial currents covering the same local times will be critical.

5 Summary

The main focus of this paper is the determination of electric currents in Jupiter's magnetodisk in the midnight-to-dawn sector. Based on Juno observations of 404 magnetodisk crossings, we first established the spatial distribution of the height-integrated perpendicular current density $I_\perp$ in the magnetodisk. Then, we decomposed $I_\perp$ into its radial (I_r) and azimuthal (I_a) components, and calculated from their divergence their respective contributions J_r and J_a to the total FACs ($J_\parallel = J_r + J_a$) connecting the magnetodisk to the two conjugate ionospheres. This led us to the following main findings:

1. I_a decreases from $\sim$2000 kA/R$_J$ at r $\sim$20 R$_J$ to $\sim$400 kA/R$_J$ at r $\sim$100 R$_J$, whereas I_r is $\sim 10^2$ kA/R$_J$ at all r.

2. J_r flows into and out of the magnetodisk inside and outside of r =60 R$_J$, respectively. After integrating J_r over the corresponding radial extent, the total into-magnetodisk

currents (25.9±6.1 MA/rad) are found to be significantly larger than the total out-of-magnetodisk currents (2.9±5.2 MA/rad).

3. Within the local time range covered, I_a decreases with increasing ϕ, leading to a J_a flowing out of the magnetodisk at all r, thus breaking the local time symmetry of the magnetosphere in this local time quadrant.

4. $J_{\parallel}$ flows out of the magnetodisk (~ -10 kA/R$_J^2$) inside r =20 R$_J$, into the magnetodisk (~ 4 kA/R$_J^2$) between 40 R$_J$ and 60 R$_J$, and again out of the magnetodisk (~ -1.5 kA/R$_J^2$) outside of 60 R$_J$. The total FACs in and out of the magnetodisk nearly exactly balance, within the error range, after integrating $J_{\parallel}$ over the whole domain of study.

5. Using the estimates of I_r from this study and radial profiles of the magnetic field B_n orthogonal to the magnetodisk and of the plasma rotation rate ω obtained in previous studies, we have been able to estimate that the radial mass transport rate in the magnetodisk is close to ∼1500 kg/s.

Acknowledgments

This work was supported by the Major Project of Chinese National Programs for Fundamental Research and Development 2021YFA0718600 (Q.G.Z.), the National Natural Science Foundation of China 42230202 (Q.G.Z), and the China Space Agency project D020301 (Q.G.Z). Michel Blanc wishes to express his gratitude to CNES for its support to his participation in the Juno mission. The authors are very grateful to NASA and to the contributing institutions that have made the Juno mission possible, and to all institutions supporting the development, operation and data analysis of the Juno/MAG instruments. Our special thanks to Dr. John E. Connerney, Principal Investigator of the MAG experiment and to the MAG team for providing data critical to this study.

Data Availability Statement

The authors acknowledge the use of NASA Planetary Plasma Interactions Node for obtaining the Juno/MAG data (https://pds-ppi.igpp.ucla.edu/search/view/?f=yes&id=pds://PPI/JNO-J-3-FGM-CAL-V1.0/DATA; also see *Connerney* [2017]). The statistical datasets can be found in *Liu et al.* [2021].

References

Al Saati, S., N. Clément, M. Blanc, Y. Wang, N. André, C. Louis, L. Lamy, P.-L. Blelly, P. Louarn, A. Marchaudon, et al. (2022), Magnetosphere-ionosphere-thermosphere coupling study at jupiter based on juno first 30 orbits and modelling tools, *Journal of Geophysical Research: Space Physics*, *127*(10), e2022JA030,586.

Arridge, C., M. Kane, N. Sergis, K. Khurana, and C. Jackman (2016), Sources of local time asymmetries in magnetodiscs, in *The Magnetodiscs and Aurorae of Giant Planets*, pp. 301–333, Springer.

Bagenal, F., A. Adriani, F. Allegrini, S. Bolton, B. Bonfond, E. Bunce, J. Connerney, S. Cowley, R. Ebert, G. Gladstone, et al. (2017), Magnetospheric science objectives of the juno mission, *Space Science Reviews*, *213*(1), 219–287.

Bonfond, B., Z. Yao, and D. Grodent (2020), Six pieces of evidence against the corotation enforcement theory to explain the main aurora at jupiter, *Journal of Geophysical Research: Space Physics*, *125*(11), e2020JA028,152.

Caudal, G. (1986), A self-consistent model of jupiter's magnetodisc including the effects of centrifugal force and pressure, *Journal of Geophysical Research: Space Physics*, *91*(A4), 4201–4221.

Connerney, J., M. Benn, J. Bjarno, T. Denver, J. Espley, J. Jorgensen, P. Jorgensen, P. Lawton, A. Malinnikova, J. Merayo, et al. (2017), The juno magnetic field investigation, *Space Science Reviews*, *213*(1), 39–138.

Connerney, J., S. Timmins, M. Herceg, and J. Joergensen (2020), A jovian magnetodisc model for the juno era, *Journal of Geophysical Research: Space Physics*, *125*(10), e2020JA028,138.

Connerney, J. E. P. (2017), Juno fluxgate magnetometer calibrated data v1.0 [data set], *NASA Planetary Data System*, https://doi.org/10.17189/1519711.

Cowley, S., and E. Bunce (2001), Origin of the main auroral oval in jupiter's coupled magnetosphere–ionosphere system, *Planetary and Space Science*, *49*(10-11), 1067–1088.

Delamere, P., and F. Bagenal (2010), Solar wind interaction with jupiter's magnetosphere, *Journal of Geophysical Research: Space Physics*, *115*(A10).

Delamere, P., F. Bagenal, and A. Steffl (2005), Radial variations in the io plasma torus during the cassini era, *Journal of Geophysical Research: Space Physics*, *110*(A12).

Grodent, D., J. Clarke, J. Kim, J. Waite Jr, and S. Cowley (2003), Jupiter's main auroral oval observed with hst-stis, *Journal of Geophysical Research: Space Physics*, *108*(A11).

Gurnett, D. A., W. S. Kurth, G. B. Hospodarsky, A. Persoon, P. Zarka, A. Lecacheux, S. Bolton, M. Desch, W. M. Farrell, M. L. Kaiser, et al. (2002), Control of jupiter's radio emission and aurorae by the solar wind, *Nature*, *415*(6875), 985–987.

Hairston, M., and T. Hill (1986), Superrotation in the pre-dawn jovian magnetosphere: Evidence for corotating convection, *Geophysical research letters*, *13*(6), 521–524.

Hill, T. (1976), Interchange stability of a rapidly rotating magnetosphere, *Planetary and Space Science*, *24*(12), 1151–1154.

Hill, T. (1979), Inertial limit on corotation, *Journal of Geophysical Research: Space Physics*, *84*(A11), 6554–6558.

Hill, T. (2001), The jovian auroral oval, *Journal of Geophysical Research: Space Physics*, *106*(A5), 8101–8107.

Hill, T., and F. Michel (1976), Heavy ions from the galilean satellites and the centrifugal distortion of the jovian magnetosphere, *Journal of Geophysical Research*, *81*(25), 4561–4565.

Khurana, K., H. Leinweber, G. Hospodarsky, and C. Paranicas (2022), Radial and local time variations in the thickness of jupiter's magnetospheric current sheet, *Journal of Geophysical Research: Space Physics*, *127*(10), e2022JA030,664.

Khurana, K. K. (1992), A generalized hinged-magnetodisc model of jupiter's nightside current sheet, *Journal of Geophysical Research: Space Physics*, *97*(A5), 6269–6276.

Khurana, K. K. (2001), Influence of solar wind on jupiter's magnetosphere deduced from currents in the equatorial plane, *Journal of Geophysical Research: Space Physics*, *106*(A11), 25,999–26,016.

Khurana, K. K., and M. G. Kivelson (1989), On jovian plasma sheet structure, *Journal of Geophysical Research: Space Physics*, *94*(A9), 11,791–11,803.

Khurana, K. K., and M. G. Kivelson (1993), Inference of the angular velocity of plasma in the jovian magnetosphere from the sweepback of magnetic field, *Journal of Geophysical Research: Space Physics*, *98*(A1), 67–79.

Kim, T. K., R. Ebert, P. Valek, F. Allegrini, D. McComas, F. Bagenal, J. Connerney, G. Livadiotis, M. Thomsen, R. Wilson, et al. (2020), Survey of ion properties in jupiter's plasma sheet: Juno jade-i observations, *Journal of Geophysical Research: Space Physics*, *125*(4), e2019JA027,696.

Kivelson, M. G., P. J. Coleman Jr, L. Froidevaux, and R. L. Rosenberg (1978), A time dependent model of the jovian current sheet, *Journal of Geophysical Research: Space Physics*, *83*(A10), 4823–4829.

Kotsiaros, S., J. E. Connerney, G. Clark, F. Allegrini, G. R. Gladstone, W. S. Kurth, B. H. Mauk, J. Saur, E. J. Bunce, D. J. Gershman, et al. (2019), Birkeland currents in jupiter's magnetosphere observed by the polar-orbiting juno spacecraft, *Nature Astronomy*, *3*(10), 904–909.

Liu, Z.-Y., Q.-G. Zong, M. Blanc, Y.-X. Sun, J.-T. Zhao, Y.-X. Hao, and B. Mauk (2021), Statistics on jupiter?s current sheet with juno data: Geometry, magnetic fields and energetic particles, *Journal of Geophysical Research: Space Physics*, *126*(11), e2021JA029,710.

Lorch, C., L. C. Ray, C. Arridge, K. Khurana, C. Martin, and A. Bader (2020), Local time asymmetries in jupiter's magnetodisc currents, *Journal of Geophysical Research: Space Physics*, *125*(2), e2019JA027,455.

McComas, D., N. Alexander, F. Allegrini, F. Bagenal, C. Beebe, G. Clark, F. Crary, M. Desai, A. De Los Santos, D. Demkee, et al. (2017), The jovian auroral distributions experiment (jade) on the juno mission to jupiter, *Space Science Reviews*, *213*(1), 547–643.

Millas, D., N. Achilleos, P. Guio, and C. Arridge (2023), Modelling magnetic fields and plasma flows in the magnetosphere of jupiter, *Planetary and Space Science*, *225*, 105,609.

Nichols, J., and S. Cowley (2022), Relation of jupiter's dawnside main emission intensity to magnetospheric currents during the juno mission, *Journal of Geophysical Research: Space Physics*, *127*(1), e2021JA030,040.

Nichols, J. D., N. Achilleos, and S. W. Cowley (2015), A model of force balance in jupiter's magnetodisc including hot plasma pressure anisotropy, *Journal of Geophysical Research: Space Physics*, *120*(12), 10–185.

Ray, L., N. Achilleos, M. Vogt, and J. Yates (2014), Local time variations in jupiter's magnetosphere-ionosphere coupling system, *Journal of Geophysical Re-*

search: Space Physics, *119*(6), 4740–4751.

Smith, E., L. Davis Jr, and D. Jones (1976), Jupiter's magnetic field and magnetosphere, in *IAU Colloq. 30: Jupiter: Studies of the Interior, Atmosp here, Magnetosphere and Satellites*, pp. 788–829.

Sonnerup, B. U., and M. Scheible (1998), Minimum and maximum variance analysis, *Analysis methods for multi-spacecraft data*, *1*, 185–220.

Southwood, D., and M. Kivelson (2001), A new perspective concerning the influence of the solar wind on the jovian magnetosphere, *Journal of Geophysical Research: Space Physics*, *106*(A4), 6123–6130.

Southwood, D. J., and M. G. Kivelson (1987), Magnetospheric interchange instability, *Journal of Geophysical Research: Space Physics*, *92*(A1), 109–116.

Szalay, J., F. Allegrini, F. Bagenal, S. Bolton, G. Clark, J. Connerney, L. Dougherty, R. Ebert, D. Gershman, W. Kurth, et al. (2017), Plasma measurements in the jovian polar region with juno/jade, *Geophysical Research Letters*, *44*(14), 7122–7130.

Thomas, N., F. Bagenal, T. Hill, and J. Wilson (2004), The io neutral clouds and plasma torus, *Jupiter. The planet, satellites and magnetosphere*, *1*, 561–591.

Vasyliunas, V. (1983), Plasma distribution and flow, inphysics of the jovian magnetosphere, edited by aj dessler.

Wang, Y., M. Blanc, C. Louis, C. Wang, N. André, A. Adriani, F. Allegrini, P.-L. Blelly, S. Bolton, B. Bonfond, et al. (2021), A preliminary study of magnetosphere-ionosphere-thermosphere coupling at jupiter: Juno multi-instrument measurements and modeling tools, *Journal of Geophysical Research: Space Physics*, *126*(9), e2021JA029,469.

Yao, Z., D. Grodent, W. Kurth, G. Clark, B. Mauk, T. Kimura, B. Bonfond, S.-Y. Ye, A. Lui, A. Radioti, et al. (2019), On the relation between jovian aurorae and the loading/unloading of the magnetic flux: Simultaneous measurements from juno, hubble space telescope, and hisaki, *Geophysical Research Letters*, *46*(21), 11,632–11,641.

Yao, Z., B. Bonfond, D. Grodent, E. Chané, W. Dunn, W. Kurth, J. Connerney, J. Nichols, B. Palmaerts, R. Guo, et al. (2022), On the relation between auroral morphologies and compression conditions of jupiter's magnetopause: Observations from juno and the hubble space telescope, *Journal of Geophysical Research: Space*

626 *Physics*, *127*(10), e2021JA029,894.

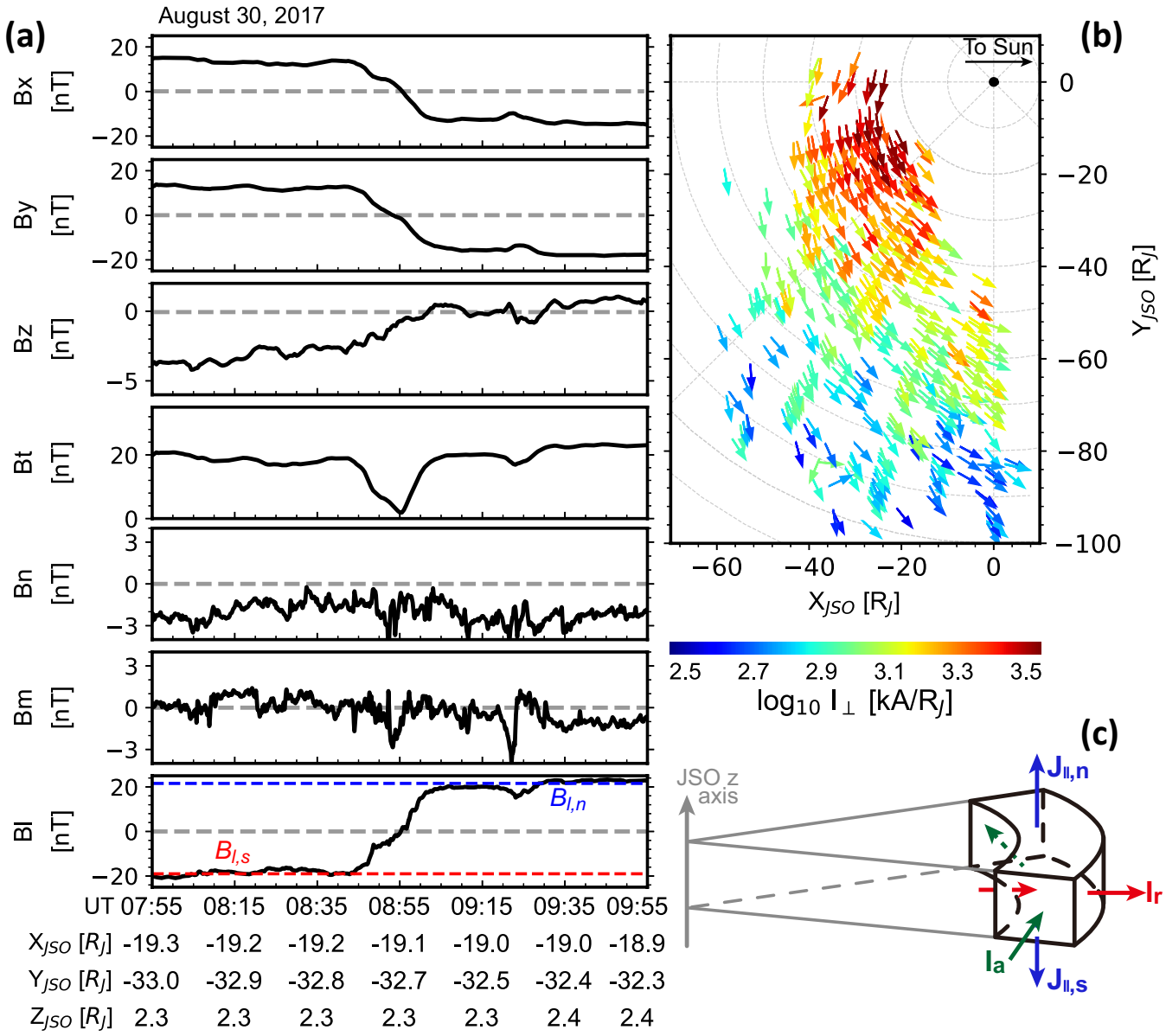

Figure 1. Juno observations of a magnetodisk crossing and the height-integrated currents in the magnetodisk. (a) Magnetic fields observed by Juno/MAG during a magnetodisk crossing on August 30, 2017. From top to bottom, the panels give the x, y, and z components in the JSO coordinates, the magnitude, and the n, m, and l components in the LMN coordinates. The blue and red lines in the bottom panel mark the values of $B_{l,n}$ and $B_{l,s}$, respectively. (b) Height-integrated perpendicular current density in the global reference frame, with the colors representing the magnitude and the short lines giving the direction. (c) Schematics showing how to calculate the field-aligned currents from the divergence of magnetodisk currents. The global reference frame is used to present the involved quantities.

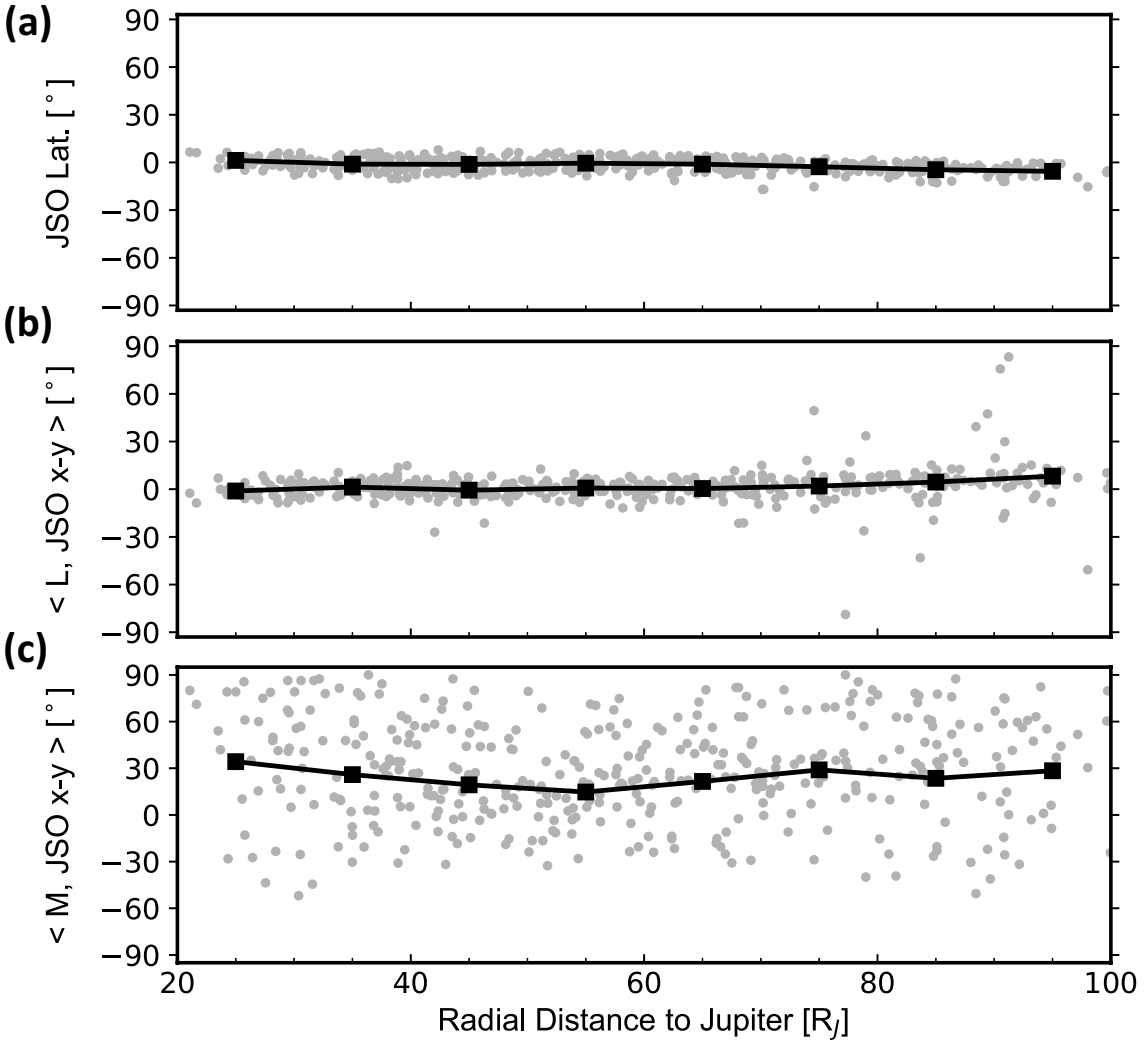

Figure 2. The geometry of the LMN coordinates. (a) The JSO latitude of the magnetodisk crossings, with the grey dots corresponding to individual crossings and the black squares representing the mean value in each radial distance bin. (b) The angle from the L axis to the JSO x-y plane. (c) The angle from the M axis to the JSO x-y plane.

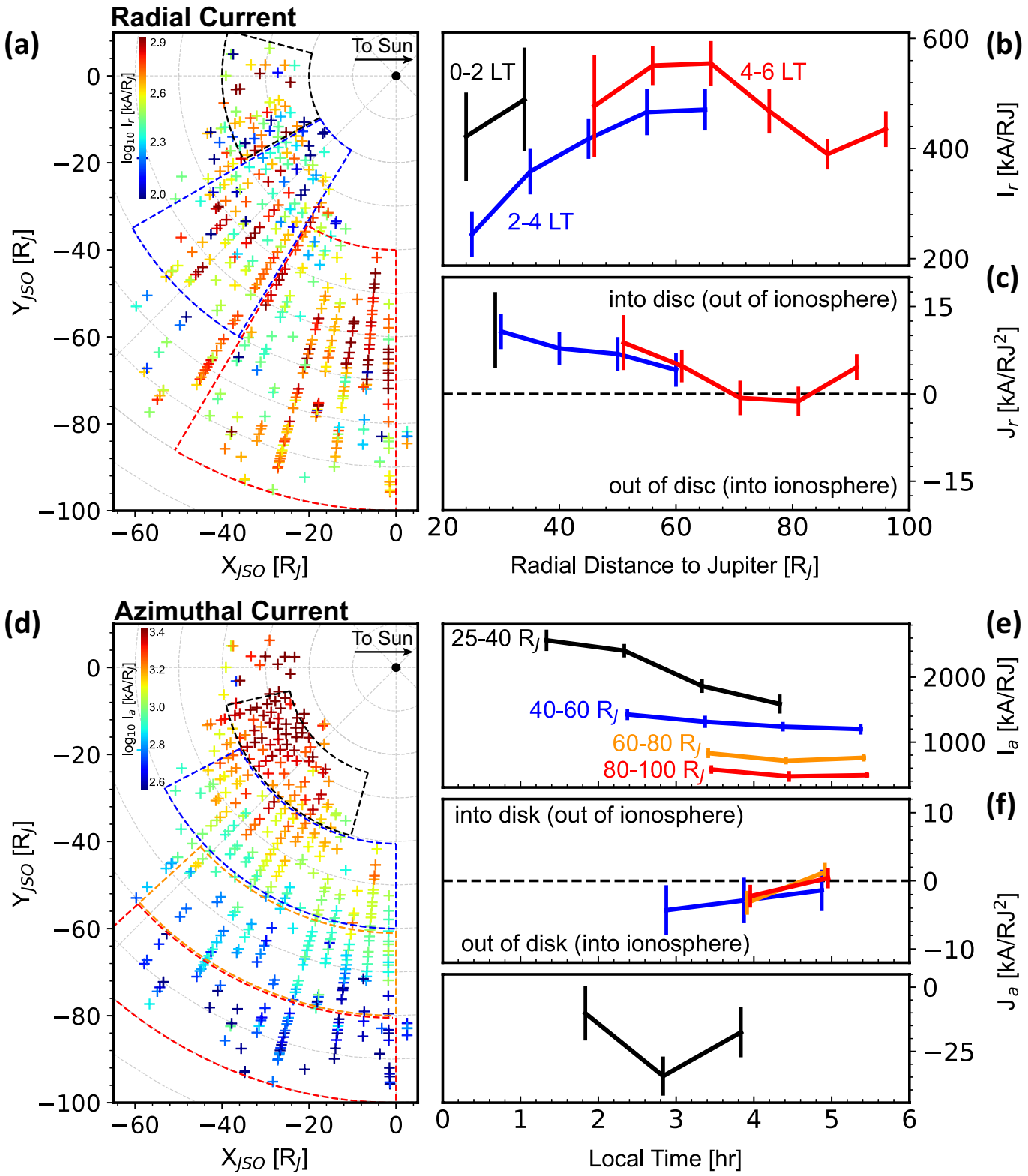

Figure 3. Height-integrated perpendicular current density and its divergence. (a) The height-integrated radial current density I_r. (b) I_r in three different local time bins. (c) The radial gradient of I_r. (d-f) Similar to panels a-c, but showing the height-integrated azimuthal current density I_a. Error bars represent standard uncertainty.

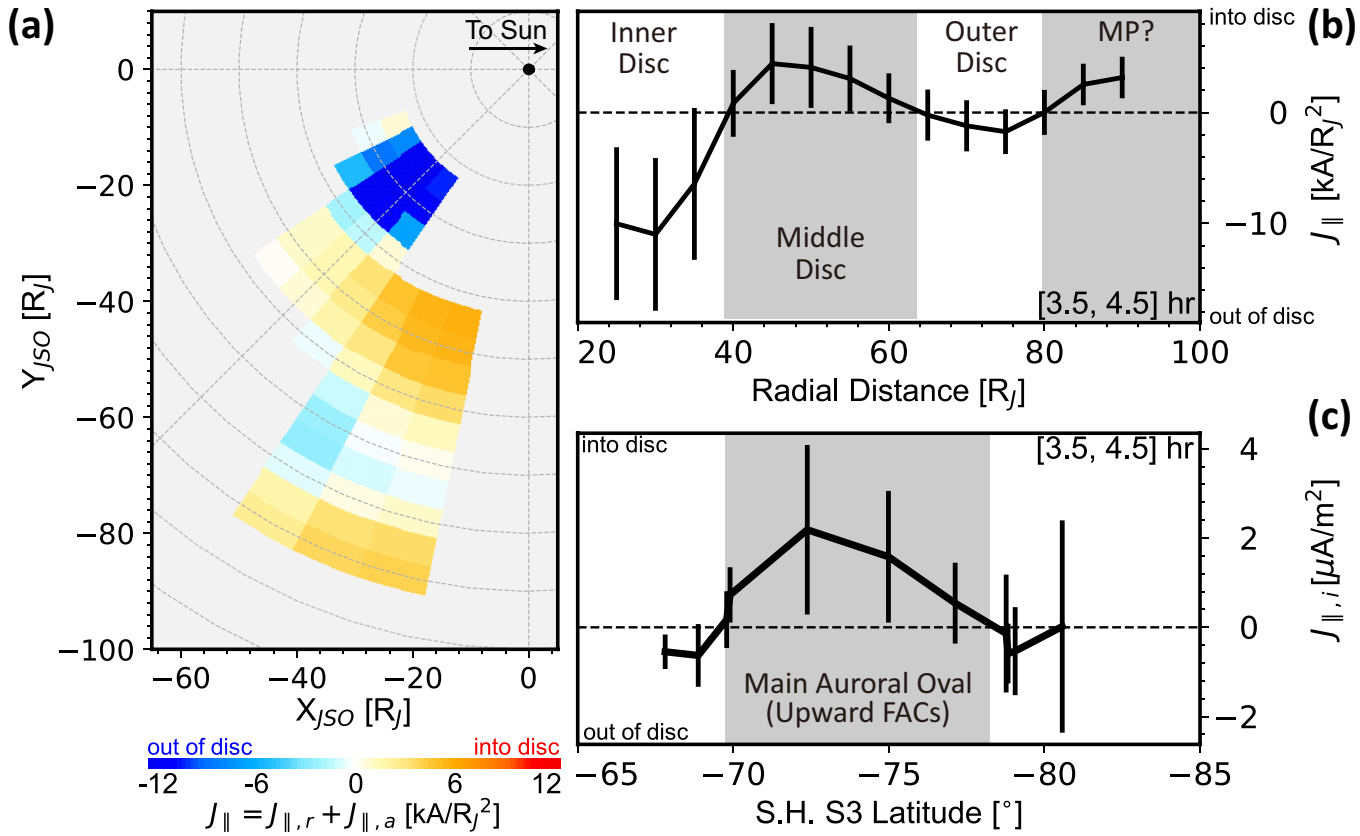

644 **Figure 4.** Field-aligned current density $J_\parallel$. (a) The JSO x-y plane distribution of $J_\parallel$. Positive
645 (warm color) and negative (cool color) values represent $J_\parallel$ flowing into the magnetodisk (out of
646 the ionosphere) and out of the magnetodisk (into the ionosphere), respectively. (b) $J_\parallel$ within 3.5
647 hr<local time<4.5 hr, as a function of the radial distance to Jupiter. (c) Similar to panel b but
648 shows $J_\parallel$ mapped to the southern ionosphere. Shadowed areas in panels b and c mark the regions
649 of positive (upward) field-aligned currents. Error bars represent standard uncertainty.

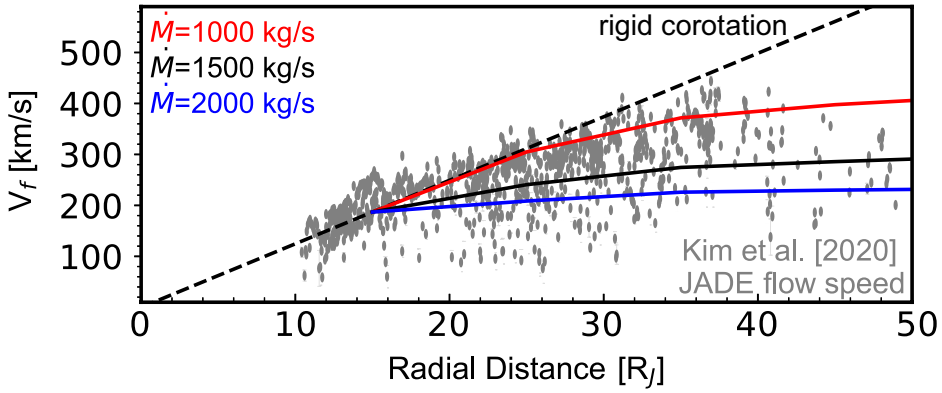

Figure 5. Radial mass transport rate. The grey dots show flow speed obtained by *Kim et al.* [2020] based on Juno/JADE ion observations. The dashed line shows rigid corotation speed. The three solid curves show the flow speed derived from Equation (5), with the red, black and blue curves corresponding to the radial mass transport rate of 1000 kg/s, 1500 kg/s and 2000 kg/s, respectively.